Environ Sci Pollut Res (2015) 22:18859–18873
DOI 10.1007/s11356-015-5032-3

RESEARCH ARTICLE

Efficient photocatalytic degradation of organic pollutants by magnetically recoverable nitrogen-doped TiO_2 nanocomposite photocatalysts under visible light irradiation

Sahar Hamzezadeh-Nakhjavani[1] · Omid Tavakoli[1] · Seyed Parham Akhlaghi[1] · Zeinab Salehi[1] · Parvaneh Esmailnejad-Ahranjani[2] · Ayyoob Arpanaei[2]

Received: 17 April 2015 / Accepted: 3 July 2015 / Published online: 24 July 2015

Abstract Preparation of novel nanocomposite particles (NCPs) with high visible-light-driven photocatalytic activity and possessing recovery potential after advanced oxidation process (AOP) is much desired. In this study, pure anatase phase titania (TiO_2) nanoparticles (NPs) as well as three types of NCPs including nitrogen-doped titania (TiO_2-N), titania-coated magnetic silica (Fe_3O_4 cluster@SiO_2@TiO_2 (FST)), and a novel magnetically recoverable TiO_2 nanocomposite photocatalyst containing nitrogen element (Fe_3O_4 cluster@SiO_2@TiO_2-N (FST-N)) were successfully synthesized via a sol–gel process. The photocatalysts were characterized by X-ray diffraction (XRD), Fourier transform infrared (FT-IR) spectroscopy, field emission scanning electron microscopy (FE-SEM) with an energy-dispersive X-ray (EDX) spectroscopy analysis, X-ray photoelectron spectroscopy (XPS), UV–vis diffuse reflectance spectroscopy (DRS), and vibrating sample magnetometer (VSM). The photocatalytic activity of as-prepared samples was further investigated and compared with each other by degradation of phenol, as a model for the organic pollutants, in deionized (DI) water under visible light irradiation. The TiO_2-N (55±1.5 %) and FST-N (46±1.5 %) samples exhibited efficient photocatalytic activity in terms of phenol degradation under visible light irradiation, while undoped samples were almost inactive under same operating conditions. Moreover, the effects of key operational parameters, the optimum sample calcination temperature, and reusability of FST-N NCPs were evaluated. Under optimum conditions (calcination temperature of 400 °C and near-neutral reaction medium), the obtained results revealed efficient degradation of phenol for FST-N NCPs under visible light irradiation (46±1.5 %), high yield magnetic separation and efficient reusability of FST-N NCPs (88.88 % of its initial value) over 10 times reuse.

Keywords Core/shell nanocomposite particles · Titania · Organic pollutants · Nitrogen-doping · Magnetic separation · Visible light · Photocatalytic degradation

Responsible editor: Santiago V. Luis

✉ Omid Tavakoli
otavakoli@ut.ac.ir

✉ Ayyoob Arpanaei
arpanaei@yahoo.com

[1] School of Chemical Engineering, College of Engineering, University of Tehran, Tehran, IranP.O. Box: 11365-4563

[2] Department of Industrial and Environmental Biotechnology, National Institute of Genetic Engineering and Biotechnology, P.O. Box: 14965-161, Tehran, Iran

Introduction

Recently, a vast number of investigations have been reported on the development of chemical and biological technologies for the degradation of organic pollutants in aqueous matrices. Efficient and novel methods such as advanced oxidation processes (AOPs) have been considered as one of the most promising technologies for the treatment of a wide range of recalcitrant materials such as organic pollutants from water and wastewater (Parsons 2004). Among the various types of AOPs, heterogeneous semiconductor photocatalysis using titania (TiO_2) as the photocatalyst has gained a lot of attention in the oxidation of organic and inorganic species (Calza et al. 2006). The importance of these photocatalysts is due to the unique properties of TiO_2, such as photochemical stability, biocompatibility, non-toxicity, remarkable photocatalytic activity, and low cost (Carp et al. 2004). Moreover, the heterogeneous photocatalytic reactions proceed at ambient

conditions and lead to the complete mineralization of several organic pollutants into harmless products such as H_2O, CO_2, and inorganic mineral ions (Wang et al. 2012). However, industrial and practical applications of TiO_2 as photocatalysts are faced with two major drawbacks.

The first main drawback is relatively large band gap of TiO_2 that allows the absorption of only a small portion of the solar spectrum together with its low quantum efficiency due to fast electron-hole recombination in the structure of TiO_2 nanophotocatalysts (Liu et al. 2010). In order to overcome the shortcoming of relatively large band gap of TiO_2 and shift the absorption edge from UV towards the visible spectral region, several attempts have been employed such as enhancing the low quantum efficiency of TiO_2 leading to electron-hole recombination (Kim and Choi 2010); narrowing the band gap by doping metal ions such as Cu, Co, Ni, Cr, Mn, Mo, Nb, V, Fe, Ru, Au, Ag, and Pt; doping with non-metals such as B, N, C, S, F, P, and I; dye sensitization; metal-ion and non-metal co-doped TiO_2; and etc. (Carp et al. 2004). Metal dopants have several disadvantages such as thermal instability and possibly secondary water contamination in the case of using toxic metals. Thus, for the application of semiconductor photocatalysis in water reclamation and purification, the more attractive option is non-metal dopants (Yap et al. 2011). Among non-metal dopants, nitrogen is one of the most promising dopants, as numerous studies have shown that nitrogen-doped TiO_2 manifests pronounced visible light photoresponsiveness (Valentin et al. 2007).

The second major challenge of TiO_2 powders is the poor separability of TiO_2 nanoparticles (NPs) from treated water. Several techniques have been proposed in order to overcome this problem. One of the most common ways to perform the separation is using sedimentation of TiO_2 NPs after pH adjustment and inducing a coagulation-flocculation process. However, after using this method, a fraction of NPs still remains in the treated water and a further micro/nanofiltration step is usually required in order to achieve a complete purification (Fernández-Ibáñez et al. 2003). The sedimentation method can be enhanced by several techniques such as immobilizing TiO_2 NPs over other support particles (e.g., activated carbon, quartz, silica gel, alumina, zeolites, optical fibers, sand, beads, glass spheres, etc.) (Dubey et al. 2008; Li et al. 2008; Yu et al. 2009). The drawbacks of such proposed techniques are drastic reductions in the photocatalytic activity of NPs because of providing very low surface areas, low mass transfer rate, and difficult distribution of immobilized particles inside the photoreactor.

Among several reported methods for separating and recycling the particles or composites from the treated water, magnetic separation provides a convenient approach by the means of applying an external magnetic field (Cano et al. 2012). The unique properties of magnetic NPs and nanocomposite particles (NCPs), such as their high surface area and catalyst loading, convenient catalyst recycling, considerable dispersion, and outstanding stability, have led to increased attention to these materials (Chi et al. 2012). In order to magnetically separate and recycle TiO_2 nanocatalysts, a variety of TiO_2/iron oxide nanocomposites have been prepared and evaluated (Xuan et al. 2008; Wang et al. 2009).

Preparation of a magnetic photocatalyst by coating TiO_2 particles onto iron oxide have been reported by Beydoun and coworkers (Beydoun et al. 2000, 2001, 2002; Beydoun and Amal 2002). This technique has been shown to provide an excellent photocatalytic activity and efficient magnetic recovery (Jing et al. 2013). Most of the magnetic NCPs containing iron oxides comprise of a core of ferrite (e.g., $NiFe_2O_4$), maghemite (γ-Fe_2O_3) or magnetite (Fe_3O_4) NPs, and a shell of TiO_2. Although the direct coating of TiO_2 on the surface of magnetic particles could protect the sensitive and unstable magnetic NPs, specially under acidic conditions against chemical corrosion, but the direct coating may lead to a photodissolution phenomenon which not only changes the properties of the magnetic oxides but also decreases the photocatalytic activity of TiO_2 (Beydoun and Amal 2002; Beydoun et al. 2002). Due to its chemical inertia, silica (SiO_2) has been proposed to be added between the magnetic particles core and TiO_2 coating to overcome the above-mentioned problems (Wang et al. 2009). The application of an intermediate layer barrier such as SiO_2 between the magnetic core and the titanium dioxide shell may lead to the avoidance of the photodissolution of iron, magnetic core stabilization, and the prevention of the magnetic core from acting as an electron-hole recombination center which would negatively affect the photoactivity of TiO_2 NPs (Beydoun et al. 2002; Abramson et al. 2009). The deposition of TiO_2 onto silica-coated iron oxide NPs has been conducted by several techniques such as impregnation, precipitation, and sol–gel (Ren et al. 2013).

Magnetic visible-active photocatalysts have been shown to be promising materials for overcoming the two fundamental drawbacks of titanium dioxide NPs that hinder TiO_2 application and development in the fields of environmental pollutants and energy sources (Wu et al. 2012). Recently, several techniques have been proposed in order to induce visible light activity and magnetic separability to TiO_2 NPs (Liu et al. 2014a, b; Zhang et al. 2014). In this study, in order to achieve the purpose of simultaneously overcoming the two mentioned drawbacks of TiO_2 NPs, four different photocatalysts based on TiO_2, including pure anatase phase TiO_2, nitrogen-doped TiO_2, TiO_2-coated magnetic silica (Fe_3O_4 cluster@SiO_2@TiO_2 (FST)), and a novel core/shell/shell structure containing nitrogen element (Fe_3O_4 cluster@SiO_2@TiO_2-N (FST-N)), were successfully fabricated by a sol–gel route followed by a calcination step. The photocatalytic activity of the as-prepared samples was investigated and compared with each other under visible light irradiation. Herein, phenol was chosen as an organic pollutant

model because of its high solubility in water and extreme toxicity (Arana et al. 2001). It is also worth mentioning that the magnetic separation method has shown to be a promising catalyst regenerating method for phenol-containing wastewaters (Chang and Tseng 2013). Finally, in the case of FST-N NCPs, the effect of key operational parameters and the reusability of the nanocomposites were evaluated.

Materials and methods

Materials

Silica-coated magnetite cluster (Fe_3O_4 cluster@SiO_2 (FS)) NCPs with an average size, core size, shell thickness, and magnetization saturation of 120±10 nm, 80±15 nm, 25± 10 nm, and 17.35 emu/g, respectively, were kindly provided by National Institute of Genetic Engineering and Biotechnology (NIGEB) (Tehran, Iran) and used without further treatment (Kalantari et al. 2013). Tetrabutyl titanate (TBOT), phenol (≥99.5 %), absolute grade ethanol, aqueous ammonia solution 25 % (*w*/*w*), and nitric acid were purchased from Merck (Germany). All chemicals used in this work were of analytical grade and were used as received without further purification. Deionized (DI) water (resistivity >18.0 MΩ cm) was used for all sample preparations.

Photocatalysts preparation

In this study, four different NPs based on TiO_2 were successfully fabricated via a sol–gel method followed by a calcination step. Firstly, for preparing pure anatase phase TiO_2 NPs, 5 mL of DI water was added to 10 mL absolute ethanol (solution A) in order to perform hydrolysis. Then under magnetic stirring, a mixture of 35 mL absolute ethanol and 10 mL TBOT (solution B) was introduced to the solution A drop-wise. The resulting solution was further refluxed at 85 °C for 2 h under vigorous stirring, leading to the formation of the sol. Afterwards, the sol was aged at room temperature for 12 h in order to obtain the gel. The gel was washed several times with ethanol, dried at 70 °C for 3 h in an oven, and ground into a fine powder. Finally, the resulting dry powder was calcined at 300, 400, and 500 °C for 2 h in a furnace with the temperature being raised at a rate of 3 °C min^{-1}; this was followed by cooling naturally to room temperature.

Nitrogen-doped TiO_2 NCPs (TiO_2-N) were synthesized using the same procedure by adding 10 mL ammonia and 2 mL nitric acid as nitrogen source to solution A.

Fabrication of magnetic NCPs also followed similar procedures. In order to synthesize the core/shell/shell structure of FST NCPs, 0.05 g of silica-coated magnetite cluster particles was added to solution A. Then in order to achieve a well-dispersed solution of magnetic NPs, the resulting solution was ultrasonicated for about 30 min.

Finally, in order to induce photocatalytic activity to the as-prepared magnetic NCPs under visible light irradiation, a novel FST-N structure was fabricated by the addition of 10 mL ammonia and 2 mL nitric acid as nitrogen source to solution A of $Fe_3O_4/SiO_2/TiO_2$ synthesis procedure.

Characterization of the as-prepared samples

The NCPs were characterized for structural, morphological, and chemical properties. The crystal structure of the as-prepared particles were characterized using X-ray diffraction (XRD, Shimadzu XRD-6000) with Cu Kα radiation (λ= 0.15418 nm) in the 2θ range of 20–80°. Fourier transform infrared (FT-IR) spectra of the samples were collected at ambient conditions using KBr pellets as diluent to determine the specific functional groups using Bruker FTIR Tensor-27 spectrometer. The size and morphology of samples were examined by field emission scanning electron microscopy (FE-SEM, Philips FEI XL30). The surface inorganic elemental compositions of the prepared photocatalysts were evaluated by energy dispersive X-ray spectroscopy (EDS, attached to FE-SEM). X-ray photoelectron spectroscopy (XPS, Kratos Axis Ultra) studies were carried out using a spectrometer with a monochromatic Al Kα excitation source (hυ=1486.71 eV) to investigate the surface chemical compositions and bonding states of the as-prepared samples and also to confirm the N incorporation in the FST-N NCPs. All binding energies were calibrated by referencing the C 1s core level at 248.6 eV of surface adventitious carbon to reduce the sample charge effect. The band gap and optical properties of the samples were recorded on UV–vis diffuse reflectance spectrophotometer (UV–vis DRS, Avaspec-2048 TEC) with an integrating sphere attachment and $BaSO_4$ was used as a reference standard. The magnetic properties of the FST-N sample were measured by a vibrating sample magnetometer (VSM, Lakeshore 7410) at room temperature.

Analysis of photocatalytic properties of the as-prepared particles

The performance of the synthesized photocatalysts were characterized by using the photocatalytic decomposition of phenol in 600 mL of an aqueous solution containing 0.8 g of photocatalysts and a phenol concentration of between 50 and 200 mg/L. The experimental setup for laboratory irradiation experiments is schematically shown in Fig. 1. All photocatalytic experiments were carried out in a batch mode 2-L cylindrical Pyrex glass photoreactor (8 cm of diameter and 40 cm of height) in which the adequate turbulency and agitation were provided by an air pump and an air distributor at ambient temperature. Unless otherwise stated, all experiments

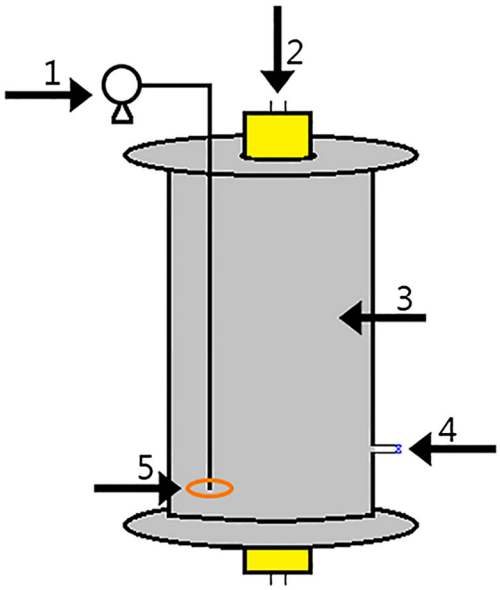

Fig. 1 Schematic diagram of experimental setup. (*1*) Air pump; (*2*) visible light source; (*3*) Pyrex reactor; (*4*) sampling valve; and (*5*) air distributor

were performed at inherent solution pH which was left uncontrolled during the reaction; the inherent solution pH was near-neutral. Solution pH was adjusted as necessary using diluted HCl or NaOH solutions. Prior to photocatalytic measurements, the suspensions were air-bubbled in dark for 30 min in order to establish complete adsorption/desorption equilibrium between the organic solution and the surface of photocatalysts. After reaching the equilibrium state, the concentration of phenol in the solution was regarded as the initial concentration. Visible light irradiation was provided by a 15-W florescent lamp with an emission maximum at λ=660 nm, located in the center of the photoreactor. Once the light was switched on, at given irradiation time intervals (every 2 h), 5 mL of the sample was collected and centrifuged at 8000 rpm for 30 min in the dark to separate particles prior to absorbance measurements. The residual concentration of phenol was monitored by observing the change in the absorbance at the maximum absorption wavelength of 500 nm using a UV–vis spectrophotometer (Specord S100, Analytik Jena GmbH, Germany), and then the concentration was calculated from a calibration curve. All runs were performed in three replicates and mean values, with standard deviations below 5 %, were quoted as results.

Recycling of FST-N NCPs

In order to investigate the reusability of FST-N NCPs under visible light irradiation, the used magnetic photocatalysts were separated with a permanent magnet, washed with ethanol for five times, dried in vacuum at 50 °C for 24 h, and then used in 10 cycles in the same reaction system.

Results and discussion

Characteristics of samples

Crystal structural characterization

Successful coating of silica-coated magnetite cluster using TiO_2 and crystalline structures of the as-prepared particles was studied using XRD analysis. Figure 2a shows the XRD patterns of TiO_2 NPs before and after calcination treatment at various temperatures. As seen, no diffraction peaks corresponding to anatase, rutile, brookite phase, or their mixtures are distinguished in diffractogram of untreated TiO_2 because of its amorphous structure. However, after calcination, the anatase peaks appeared (JCPDS File No. 21-1272), indicating that upon calcination crystallites of anatase are mainly formed from the amorphous TiO_2 NPs. The diffraction peaks became sharper with calcination temperature increasing from 300 to 400 °C, leading to crystallinity enhancement of the NPs. When the samples were calcined at 500 °C, the peak intensities of anatase decreased, and a small peak at 2θ=27.4 corresponding to the (1 1 0) plane diffraction of rutile TiO_2 (JCPDS File No. 21-1276) was found. This result indicated that a fraction of anatase phases was transformed into rutile phases. The percentage of anatase phase is calculated using the equation $A(\%)=100 / \{1+1.265(I_R/I_A)\}$ where I_R is the intensity of the reflection (1 1 0) of the rutile phase and I_A is the intensity of the anatase peak (1 0 1) signal (Demir et al. 2015). According to the XRD patterns, after increasing the calcination temperature from 400 to 500 °C, almost 8 % of the pure anatase phase was transformed into the rutile phase. While a few studies have examined the photocatalytic activity of brookite (JCPDS File no. 29-1360) TiO_2 (Paola et al. 2008), anatase phase is proved to have higher photocatalytic activity than amorphous and rutile TiO_2 (Li et al. 2005). Upon illumination, the movement of electrons in rutile phase is much slower than the anatase which provides more chances for electron/hole pair recombination and may lead to lower photocatalytic activity of NCPs (Hurum et al. 2005). Furthermore, according to the literature, iron oxide-containing NCPs may rapidly transform to antiferromagnetic α-Fe_2O_3 and lose their magnetic response during heat treatment process above 400 °C (Liu et al. 2011). Therefore, to avoid any adverse effect on the photocatalytic and magnetic properties of the as-synthesized NCPs, subsequent preparation experiments were conducted with a 400 °C calcination temperature. However, for further verification of the above hypothesis, the photocatalytic degradation performance of FST-N NCPs calcined at various temperatures was subsequently investigated and compared. Figure 2b demonstrates the multi-component diffractograms of calcined magnetic silica (Fe_3O_4 cluster@silica), FST NCPs before and after calcination treatment, and also the calcined FST-N NCPs. As stated above, all calcination treatments were

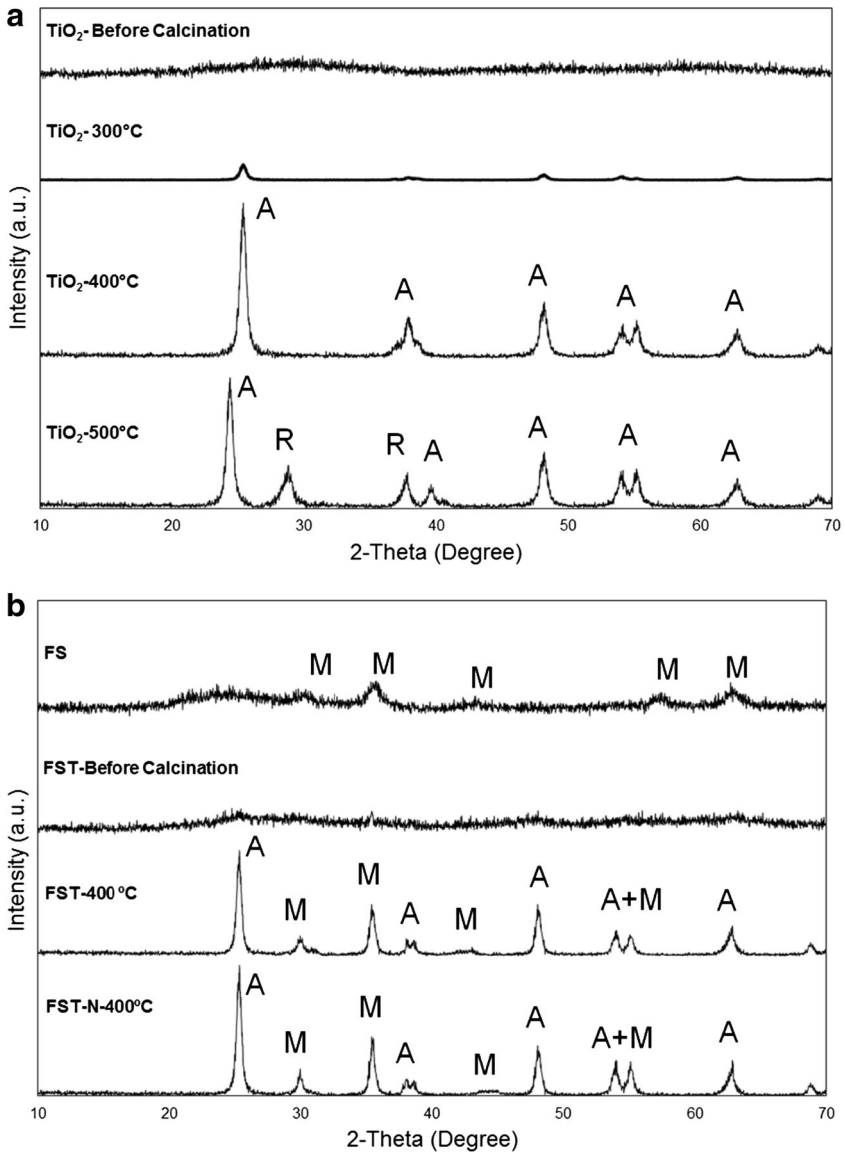

Fig. 2 XRD diffractogram of **a** TiO_2 NPs before and after calcination at various temperatures and **b** multicomponent FS, FST before and after calcination, and FST-N NCPs

performed at 400 °C. Before calcination, all diffraction peaks of FST NCPs can be perfectly indexed to the magnetite phase of Fe_3O_4 (JCPDS File No. 19-0629). Moreover, no peaks of SiO_2 (JCPDS File No. 20-1050) and none of the TiO_2 phases peaks could be observed in the XRD pattern of FST NCPs revealing the amorphous structure of the formed shells over the magnetic core. The XRD pattern of FST NCPs before calcination shows an obvious broad peak at around $2\theta=25°$, which is generally considered as the peak of amorphous silica (Deng et al. 2007). After calcination at 400 °C for 2 h, the appearance of relatively strong and sharp diffraction peaks revealed that the amorphous TiO_2 in the structure of FST NCPs has become crystalline and transferred to the anatase phase, confirming the successful TiO_2 coating and synthesis of the crystalline core/shell structure via the sol–gel method. Moreover, after the calcination step, it is obvious that the phase of Fe_3O_4 has been transformed from magnetite to hematite (JCPDS File No. 33-0664), leading to a decrease in its magnetic properties. According to Fig. 2b, N doping does not cause a change in the crystallite structure of FST NCPs. Comparing to the diffractogram of FST samples, no detectable dopant-related peaks and broadening or shifting of the peaks could be observed in FST-N diffractogram. This might be due to the low content of interstitial or substitutional N in the N-doped sample that the crystallinity change caused by N can be neglected.

FT-IR spectroscopy

The FT-IR spectra of pure and nitrogen-doped TiO_2 samples and FST and FST-N NCPs are shown in panels a and b of Fig. 3, respectively. Two peaks located at 3375 cm^{-1} (Fig. 3a) and 3194 cm^{-1} (Fig. 3b) were assigned to the stretching vibration of hydroxyl group physi-sorbed on the surface of structures, while two peaks located at 1633 cm^{-1}

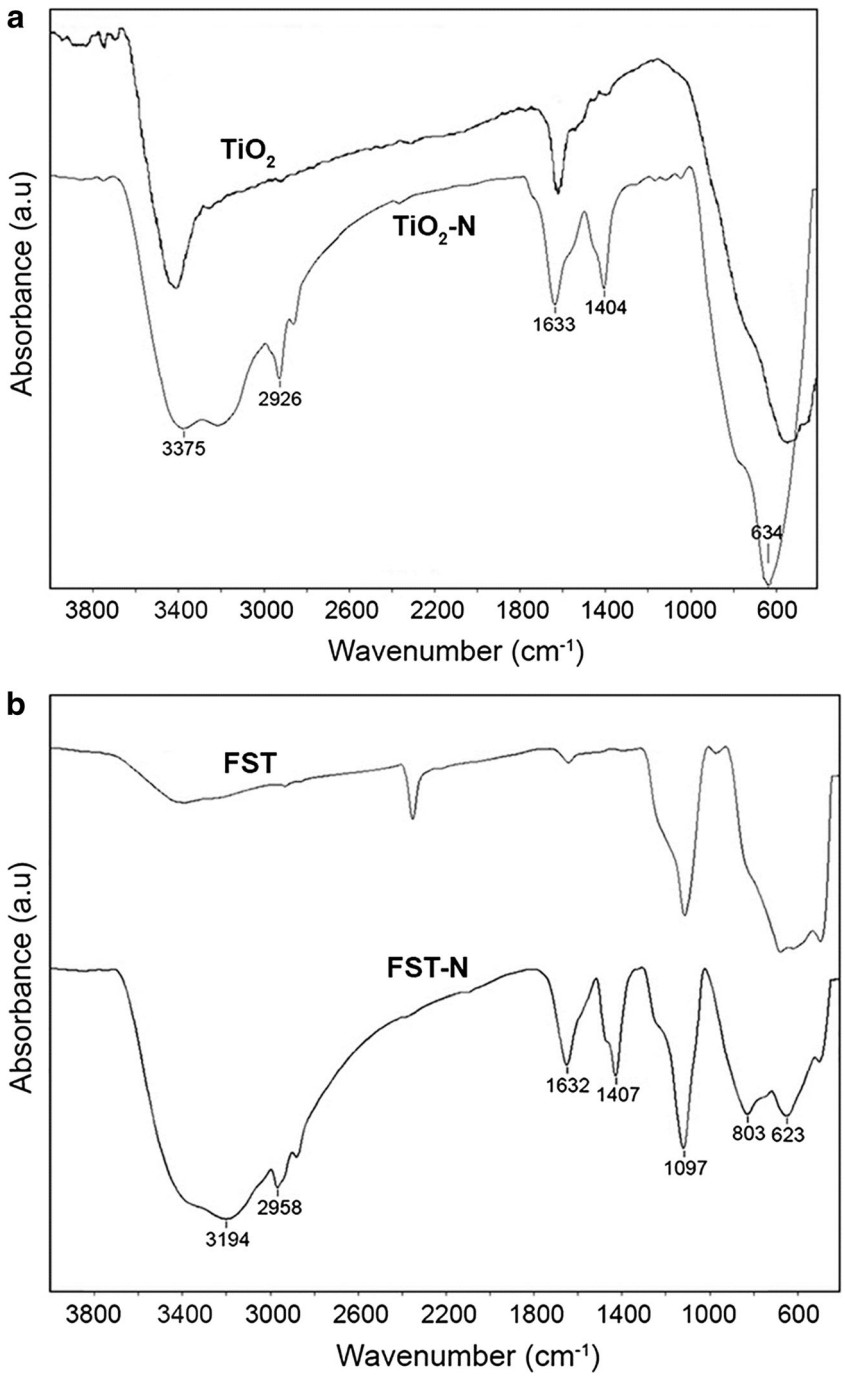

Fig. 3 FT-IR spectra of calcined **a** TiO_2 and TiO_2-N samples and **b** FST and FST-N NCPs at 400 °C

(Fig. 3a) and 1632 cm^{-1} (Fig. 3b) were related to O–H bending of dissociated or molecularly adsorbed water molecules (Shao et al. 2008; Xu et al. 2008; Hu et al. 2010). Additionally, the stronger intensity of these two absorption bands in both nitrogen-doped samples indicates that the nitrogen-doped samples have more surface adsorbed water and hydroxyl groups which lead to their higher photocatalytic activities. The two low frequency bands at 634 cm^{-1} (Fig. 3a) and 623 cm^{-1} (Fig. 3b) corresponded to the vibration of Ti–O–Ti bonds and the peaks at 2926 cm^{-1} (Fig. 3a) and 2958 cm^{-1} (Fig. 3b) could be ascribed to the C–H stretching vibrations (Swan et al. 1981; Shao et al. 2008). In Fig. 3b, the peak at 1097 cm^{-1} could be assigned to the C-O-C asymmetric stretch (Kumar et al. 2006). It is reported that the signal at the wavenumber 803 cm^{-1} could be related to the symmetric vibration of Si–O–Si (Ding et al. 2000; Jung and Park 2000). Finally, the presence of two peaks at 1404 cm^{-1} (Fig. 3a) and 1407 cm^{-1} (Fig. 3b) is attributed to the N-H bending, suggesting the substitution of nitrogen atoms into the structure of TiO_2 network (Matsumoto et al. 2007; Xu et al. 2008; Geng et al. 2009).

FE-SEM/EDX analysis

The morphology and size of the samples were characterized by FE-SEM analysis. Figure 4 shows the FE-SEM images of TiO_2, TiO_2-N, Fe_3O_4 cluster@SiO_2, FST, and FST-N samples. The as-prepared samples were found to be almost spherical in shape with a slight agglomeration. In typical samples as shown in Fig. 4, the average particle size was measured as 104.74 nm for TiO_2, 131.31 nm for TiO_2-N, 210.94 nm for Fe_3O_4 cluster@SiO_2, 250.77 nm for FST, and 287.75 nm for FST-N NCPs. Based on these values, the TiO_2 shell thickness can be estimated 24.6 and 48.3 nm for FST and FST NCPs, respectively.

Table 1 shows the results of EDX analysis as obtained from EDX spectra (figure not shown). The result of EDX elemental analysis of the as-synthesized samples reveals the appearance of Ti, O, Si, and Fe peaks, indicating that they were mainly composed of these elements while the characteristic peak for nitrogen was not evident. Therefore, EDX analysis may not be suitable for the detection of low concentrations of N and further analysis namely XPS was needed to verify the success of the doping process.

Table 1 Physicochemical properties of the as-synthesized samples

Particle	Crystallite size (nm)	Surface element content (wt%)					Band gap
		Ti	O	Si	Fe	N	
TiO_2	104	69.88	30.11				3.18
TiO_2-N	131	80.18	19.82			BLQ	2.78
FST	250	58.19	31.89	5.55	4.37		3.05
FST-N	287	59.98	29.51	6.37	4.14	BLQ	2.81

BLQ below the limit of quantification

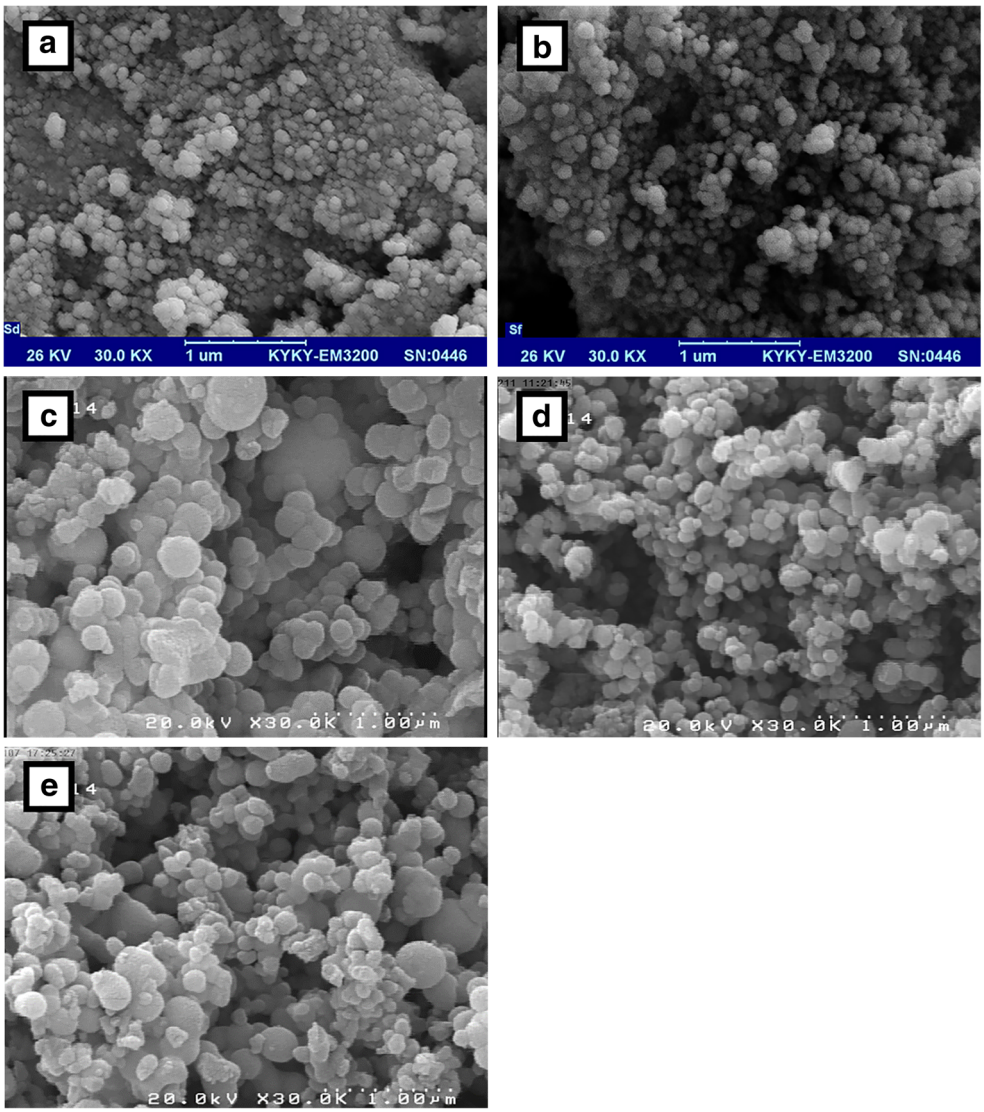

Fig. 4 FE-SEM image of **a** TiO_2; **b** TiO_2-N; **c** FS; **d** FST; and **e** FST-N

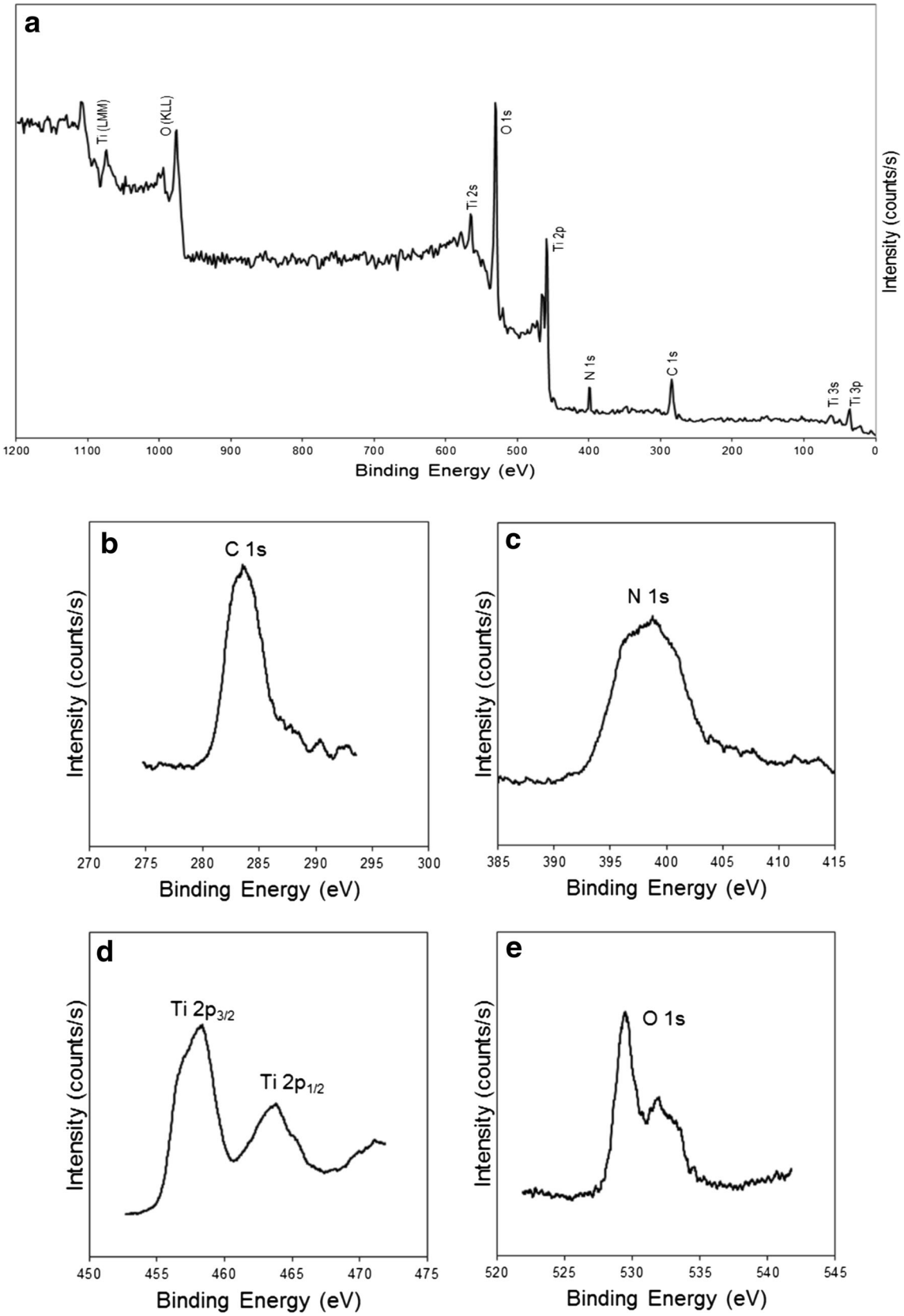

Fig. 5 X-ray photoelectron spectra of FST-N **a** survey spectrum; **b** C 1s peak; **c** N 1s peak; **d** Ti 2p peak; and **e** O 1s peak

XPS analysis

The surface chemical composition of the FST-N sample and its dopant concentration was analyzed by XPS spectroscopy. Figure 5a shows the typical full survey spectrum of the FST-N, which clearly indicated that the surface of the as-synthesized samples was of high purity and mainly composed of C, Ti, O, and N elements. It is worth noting that as XPS is a highly surface-specific technique with a typical analysis depth of ~10 nm, herein the peaks of core elements (i.e., Fe and Si) could not be distinguished. This is in good agreement with the results obtained by FE-SEM and EDX. The high-resolution scan over C 1s, N 1s, Ti 2p, O 1s, and spectral regions are shown in panels b−e of Fig. 5, respectively. The observed C 1s peak at 284.6 eV (Fig. 5b) is assigned to the adventitious elemental carbon originating from the XPS instrument or carbon residues from the organic precursor (Treschev et al. 2008). As shown in Fig. 5c, the main N 1s core level peak located at around 399 eV confirms the incorporation of nitrogen into the FST lattice (Sakthivel et al. 2004). The atomic concentration of nitrogen element was calculated using relative sensitivity factor (RSF) and was found to be about 0.61 at.%. The observed N 1s peak can be attributed to O-Ti-N linkages (Burda et al. 2003), indicating the bonding of N atoms to Ti atoms and replacement of lattice oxygen in the TiO_2. This is further supported by the results of the XPS spectra for the Ti 2p region. Figure 5d shows the Ti $2p_{3/2}$ and $2p_{1/2}$ peaks at 458.3 and 464 eV, respectively, which are attributed to the Ti 2p peaks of O–Ti–O in TiO_2 (Sathish et al. 2005). Comparing to the Ti $2p_{3/2}$ binding energies reported for pure TiO_2 (Chen and Burda 2004), the observed Ti $2p_{3/2}$ core level shows a slight shift to the lower binding energies, revealing covalency between the Ti and N bond and further formation of O-Ti-N bonds by partially substituting the O atom in the TiO_2 lattice which considerably modified FST lattice due to N-substitution (Devi and Rajashekhar 2011). The high-resolution scan of O 1s region is shown in Fig. 5e. The peak located at 529.8 eV can be attributed to the Ti-O bonds of the TiO_2 lattice (Gorska et al. 2008), while the peak at 531.8 eV reveals the presence of surface hydroxyl groups (OH) resulting mainly from the chemisorbed water (Cheng et al. 2012), which was previously confirmed by FT-IR analysis.

UV–vis DRS analysis

Figure 6 depicts the UV–vis absorbance spectra of TiO_2, TiO_2-N, FST, and FST-N NCPs in the range of 300–700 nm. As shown in Fig. 6, TiO_2-N and FST-N samples exhibited remarkable red shift of absorption edge to the visible light region which is the typical absorption property of nitrogen-doped TiO_2 (Lindgren et al. 2003). Based on the optical absorption edge obtained from the UV–vis DRS, the respective band gap energies (E_g) were calculated using the Kubelka-Munk method (Serpone et al. 1995) and are shown in the inset of Fig. 6 and listed in Table 1. The reduction in band gap of N-doped photocatalysts is mainly attributed to the substitution of the lattice oxygen by nitrogen in the lattice of titania (as confirmed by XPS analysis), which leads to band gap narrowing by the mean of hybridization of N 2p and O 2p orbitals in anatase TiO_2. Thus, incorporation of nitrogen into the lattice of TiO_2 and FST sample leads to sufficient separation of photogenerated holes and electrons and subsequent visible-driven photocatalytic activity of NCPs.

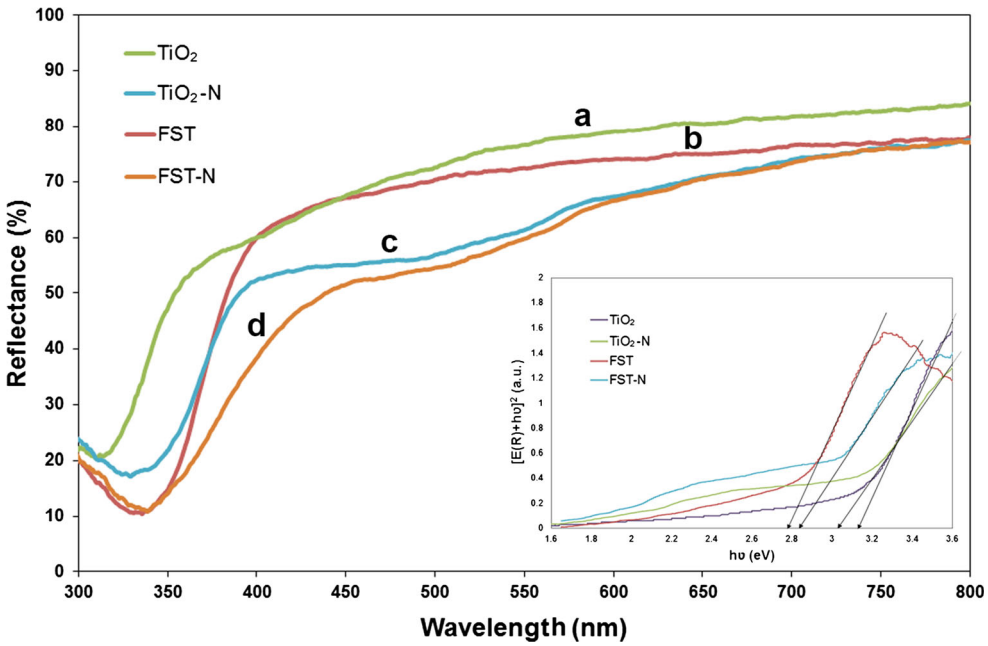

Fig. 6 UV–vis diffuse reflectance spectra of (*a*) TiO_2, (*b*) TiO_2-N, (*c*) FST, and (*d*) FST-N. The *inset* shows the corresponding Kubelka-Munk transformed reflectance spectra

VSM analysis

The magnetic properties of the FST, FST-N, and FS core were measured by VSM, as shown in Fig. 7. The maximum saturation magnetization (M_S) of the FS, FST, and FST-N NCPs were measured 17.35, 4.26, and 3.68, respectively. As there were no Fe_2O_3 characteristic peaks (2θ=24.28°,33.26°, 35.76°, 41.10°, 49.58°, and 54.20°) (Gao et al. 2011) observed in the XRD patterns of FST and FST-N NCPs, the decrease of the magnetic saturation of the FS core could be attributed to the contribution of the volume of the non-magnetic coating layer to the total sample volume. No hysteresis phenomenon was found, and the obtained remanent magnetization (M_r) and coercivity (H_C) of the magnetic samples were negligible and close to zero, indicating the superparamagnetic behavior of the synthesized NCPs at room temperature. The inset of Fig. 7 demonstrates the magnetic separation operation in which upon application of an external magnetic field, the turbid suspension of FST-N magnetic nanoparticles in treated wastewater becomes transparent within 60 s. Therefore, the synthesized magnetic NCPs can be almost completely recovered with no diminishing in both magnetic property and photocatalytic activity when an external magnetic field is applied.

Photocatalytic degradation

Photocatalytic activity of the four as-synthesized samples under visible light illumination

Figure 8 illustrates the photocatalytic activity of the four synthesized samples (0.8 g/L) by degradation of phenol (C_0= 100 mg/L), as an organic pollutant model under visible light irradiation. As shown in Fig. 8, after 480 min of visible light irradiation, no photocatalytic activity was observed for pure TiO_2 and FST samples. This phenomenon could be attributed to the wide band gap of anatase TiO_2, which not only limits the application of TiO_2 under visible light irradiation but also leads to the recombination of electrons and holes of the semiconductor that is unfavorable to the photocatalytic activity. After successful doping of TiO_2 and FST samples using ammonia and nitric acid as the nitrogen source, the samples have shown to be effective in degrading phenol in aqueous solutions. Thus, nitrogen-doping which leads to a narrower band gap energy (~2.7 eV) can effectively reduce the recombination of electron and holes and enhance photocatalytic activity (Wang et al. 2010). On the other hand, as the FT-IR analysis demonstrated, after doping nitrogen in the structure of samples, the intensity of the two absorption bands corresponding to O–H bending of dissociated or molecularly adsorbed water molecules in the FT-IR spectra of the nitrogen-doped samples become stronger. This result is mainly attributed to the presence of more adsorbed water and hydroxyl groups in the structure of N-doped NCPs, which is in a good agreement with results reported in the literature (Cheng et al. 2012). The presence of more hydroxyl groups in the structure of photocatalysts causes an enhancement in the separation efficiency of electron/hole pairs by trapping electrons. It may also lead to the formation of more reactive oxidative species such as hydroxyl radicals (•OH), which are highly capable in the oxidation process and consequently results in better photocatalytic activity. Moreover, the pumped air in the system contains oxygen which adsorbed on the surface of TiO_2 and prevents the recombination process by trapping the conduction band electrons with the formation of superoxide radical ions,

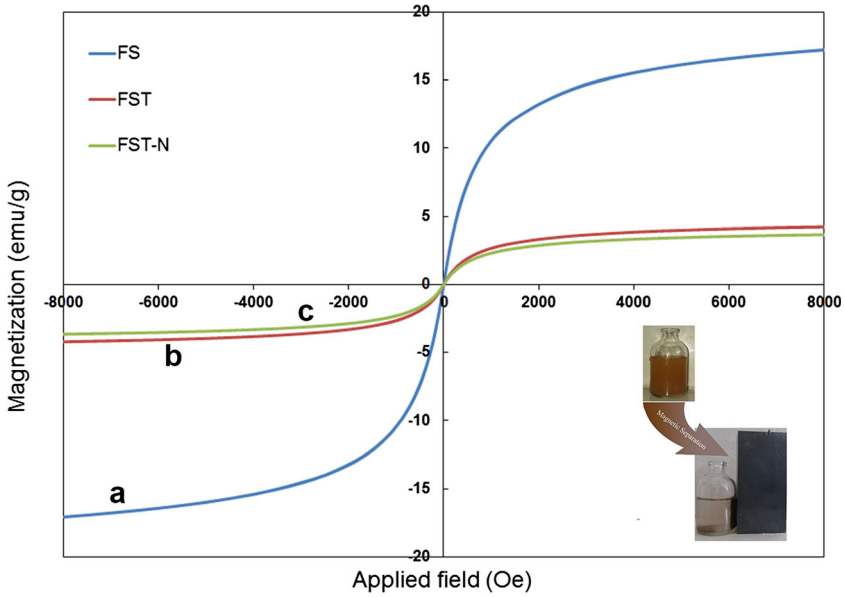

Fig. 7 Magnetic hysteresis loops of magnetic (*a*) FS, (*b*) FST, and (*c*) FST-N. The *inset* illustrates the recycling process of FST-N NCPs samples using a permanent magnet

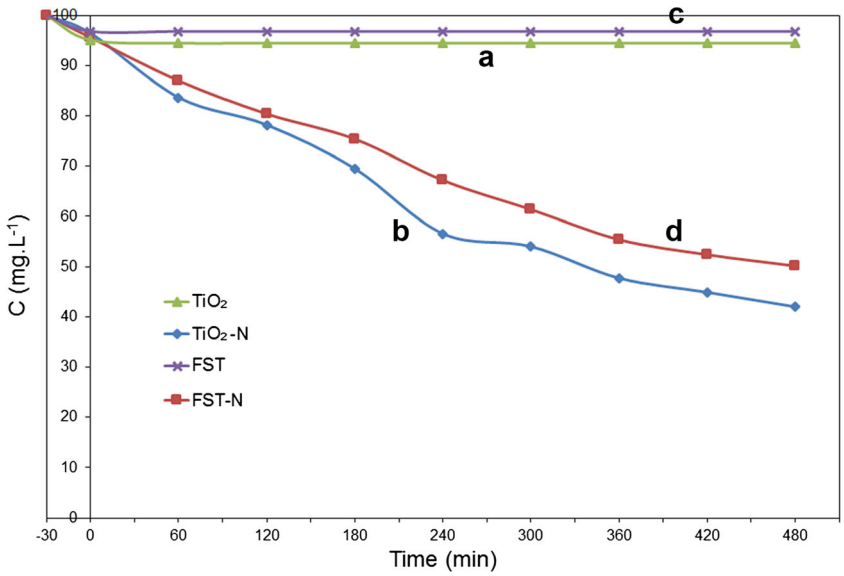

Fig. 8 Photocatalytic degradation of phenol using (*a*) TiO_2, (*b*) TiO_2-N, (*c*) FST, and (*d*) FST-N. (C_0=100 mg/L; photocatalyst dosage, 0.8 g/L; pH, near-neutral)

$O_2^{\bullet-}$. The formation of this superoxide radical ion can result in the formation of more reactive oxygen species (ROS) like peroxide radicals. The degradation efficiency of TiO_2-N and FST-N were measured as 55±1.5 and 46±1.5 %, respectively. The lower photocatalytic activity of FST-N compared to TiO_2-N particles could be attributed to the larger particle size and subsequent lower surface area of FST-N NCPs (287.75 versus 131.31 nm) (Wang et al. 1997). However, as the separability of photocatalysts from treated wastewater in practical wastewater treatment systems is of the utmost importance, FST-N magnetic NCPs were chosen for the subsequent phenol degradation studies.

Effect of calcination temperature

As stated in XRD analysis section, calcination temperature has a drastic effect on the crystal phase structure of the photocatalysts. Moreover, the calcination temperature highly affects the content of carbonaceous species and also the incorporation of nitrogen into the TiO_2 lattice (Wang et al. 2011a, b). Therefore, the photocatalytic degradation of phenol (C_0= 100 mg/L) in the presence of FST-N NCPs (0.8 g/L) which were calcined at different temperatures (300, 400, and 500 °C) was investigated under visible light illumination. The influence of calcination temperature on phenol photocatalytic degradation by the Vis/FST-N process is shown in Fig. 9a. The obtained results revealed that the highest phenol degradation efficiency (46±1.5 %) was achieved by FST-N NCPs calcined at the temperature of 400 °C. Previously, the photocatalytic activity of amorphous phase titania was reported (Lettmann et al. 2001). Herein, although the lowest degradation efficiency (17±1.5 %) was achieved by the amorphous phase FST-N NCPs calcined at the temperature of 300 °C, its capability of degrading phenol under visible light illumination is considerable. According to the XRD results, after increasing the calcination temperature up to 400 °C, crystallites of anatase are mainly formed from the amorphous samples and lead to the highest photocatalytic activity. Results in Fig. 9a reveal that the photocatalytic activity of FST-N NCPs decreases from 46±1.5 to 32±1.5 % with increasing calcination temperature from 400 to 500 °C. This reduction in activities of NCPs can be justified due to the agglomeration of NCPs, increase in crystallite size of NCPs and subsequent specific surface area reduction, limited amount of adsorbed water, and increasing the rutile phase percent (Behnajady et al. 2011). Moreover, the substituted nitrogen atoms in the lattice of FST-N NCPs may have been partially substituted by oxygen atoms with an increase in calcination temperature (Wang et al. 2005). It is worth mentioning that at calcination temperatures higher than 500 °C, Fe was found to diffuse into the TiO_2 coating and enhances the possibility of pseudobrookite (Fe_2TiO_5) phase formation at the iron oxide/titania interface, which may lead to further photocatalytic activity reduction (Beydoun et al. 2002). Therefore, further investigations on the photocatalytic activity as discussed in the following sections were focused on FST-N NCPs calcined at the temperature of 400 °C.

Effect of pH

The pH of the aqueous solution in which phenol is dissolved has a major effect on the photocatalytic degradation of phenol as the surface charge on the semiconductor particles, adsorption and dissociation of phenol, the size of the aggregates formed, and oxidation potential of the valence band are all pH dependent (Venkatachalam et al. 2007). On the other hand, phenol-containing industrial wastes can be discharged at various pH levels. Therefore, a series of experiments were carried out to investigate the influence of pH on the degradation

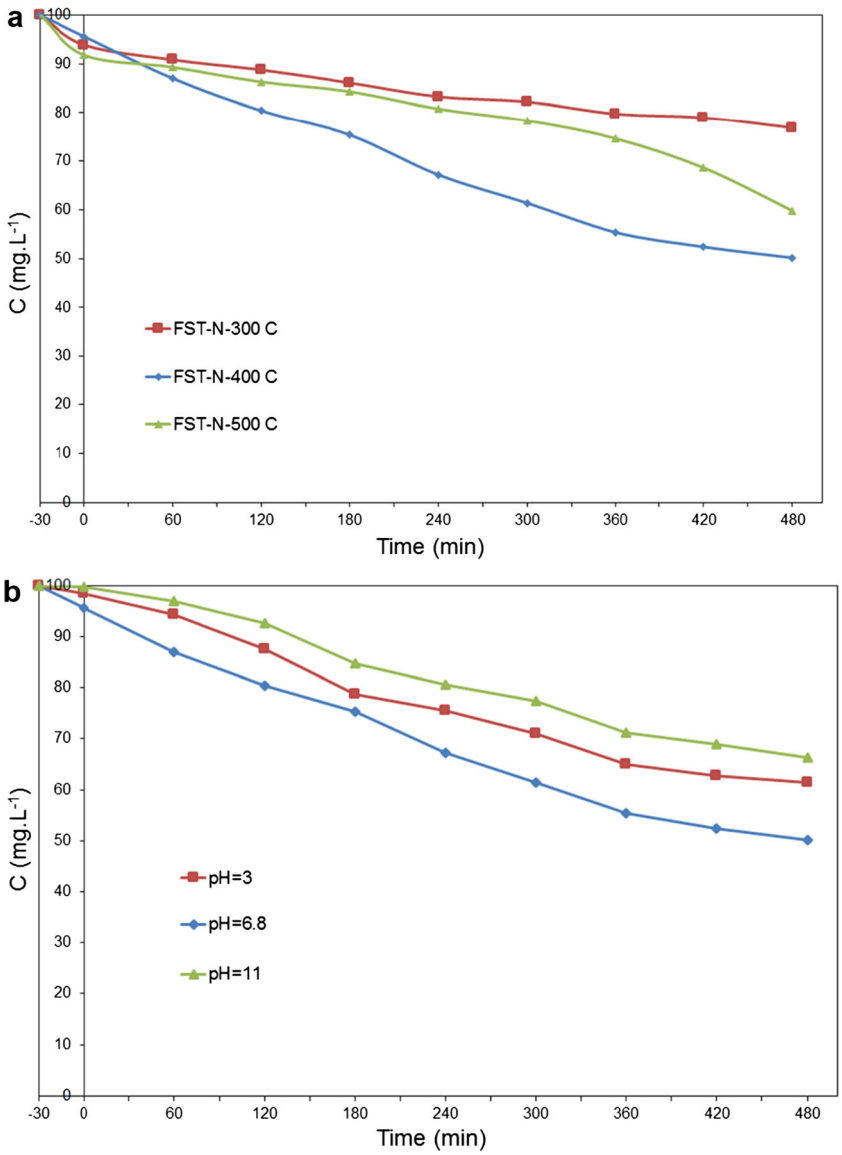

Fig. 9 Effect of **a** FST-N calcination temperature and **b** solution pH on photocatalytic degradation of phenol

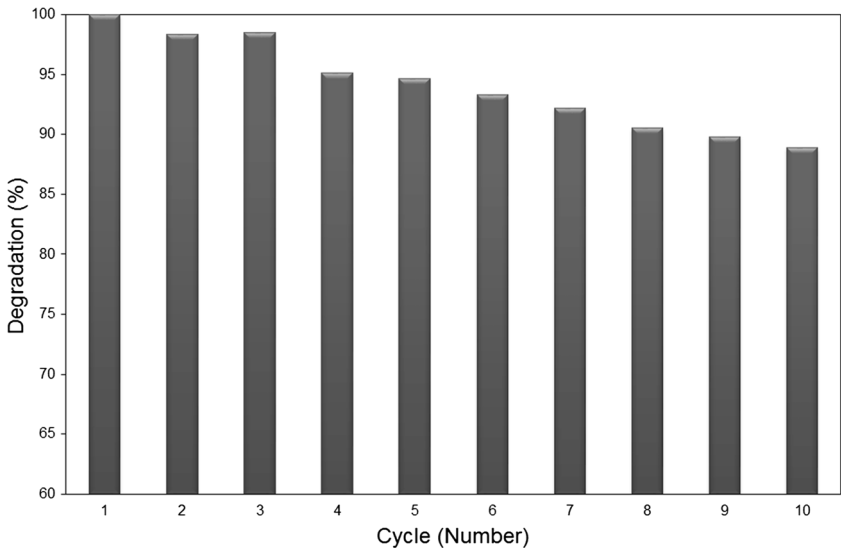

Fig. 10 Photocatalytic degradation efficiency of phenol over FST-N NCPs after repetitive use

efficiency of phenol by varying the initial pH from 3 to 11. The effect of solution pH on the phenol (C_0=100 mg/L) degradation efficiency under visible light irradiation using the FST-N NCPs (0.8 g/L) calcined at 400 °C is presented in Fig. 9b. Degradation percent after 480 min irradiation were 37±1.5, 46±1.5, and 33±1.5 % at pH 3, 7, and 11, respectively. The effect of pH on phenol degradation can be explained by taking into consideration the properties of both FST-N NCPs and phenol at different pH levels. As an amphoteric material, the FST-N NCPs surface is positively charged at a pH lower than point of zero charge (pzc) and negatively charged at a pH higher than pzc. In aqueous solutions, positive ($TiOH^{2+}$), neutral (TiOH), and negative (TiO^-) surface hydroxyl groups are formed on FST-N NCPs. The pzc of FST-N was determined to be at pH 5.9 using Malvern Nano-ZS Zetasizer. Therefore, FST-N was positively charged at pH 3, while negatively charged at pH 7 and 11. On the other hand, phenol can be considered as a weak acid with a pK_a value of 9.89 (Sanchez et al. 1995). Therefore, for pH values below 9.89, the predominant specie in solution is the molecular form of phenol, and for pH values above that, the aromatic ring becomes partially negatively charged by means of the hydroxyl group ionization and phenol deprotonates yielding negatively charged phenolate species. In basic pH range (pH=11), both phenol and FST-N NCPs acquire negative charge and hence electrostatic repulsion between FST-N and phenol retards the degradation efficiency. In neutral to weak alkaline media (pH=7), TiO^- (the predominant species on TiO_2 surface) and neutral molecular form of phenol are linked together through hydrogen bonding, which increases the phenol adsorption on the surface of photocatalyst and therefore enhances the degradation efficiency (Jing et al. 2011). Additionally, the obtained lower photocatalytic efficiency in acidic medium (pH=3) comparing to near-neutral condition could be ascribed to the higher concentration of hydroxyl radicals generated in near-neutral reaction solutions (Wang et al. 2011a, b) and hydroxyl radical scavenging of H^+ ions (Lucas and Peres 2006).

Study of reusability of FST-N nanocomposite photocatalyst

The reusability of catalysts is an important economical factor because it allows multiple usages and therefore leads to cost reduction. Moreover, the complete removal of catalysts from treated wastewater is also necessary in order to prevent an additional contamination. Thus, the reusability of TiO_2 nanocomposites must be considered as an important factor in order to make heterogeneous photocatalysis technology practical for industrial applications.

The reusability of FST-N sample was monitored by evaluating its photocatalytic activity over 10 cycles reuse. Figure 10 indicates that after 10 successive cycles under visible light irradiation, the degradation rate of phenol was still 88.88 % of its initial value, indicating that FST-N samples possess excellent photocatalytic stability and reusability properties. Herein, the photocatalyst deactivation may be attributed to the poisoning of the photocatalyst surface, which is caused by intermediates that adsorb strongly onto the surface of the NCPs and occupy the active sites on the surface of the catalysts.

Conclusions

In summary, herein four TiO_2-based photocatalysts including a novel visible-active magnetically separable nanocomposite (FST-N) with high crystalline TiO_2 shell were successfully fabricated via sol-gel methodology. The synthesized nitrogen-doped samples exhibited efficient photocatalytic activity in terms of phenol degradation under visible light irradiation, while undoped samples were almost inactive under same operating conditions. The sample characterization results revealed that the efficient visible light photocatalytic activity of TiO_2-N and FST-N samples could be attributed to the incorporation of nitrogen into the TiO_2 lattice which causes narrower band gap and enhancement in photogenerated charge separation rate and also their higher content of surface hydroxyl groups. Under near-neutral conditions, phenol degradation studies revealed that the lowest degradation efficiency (17±1.5 %) was achieved by the amorphous phase FST-N NCPs calcined at the temperature of 300 °C, while the highest phenol degradation efficiency (46±1.5 %) was achieved by FST-N NCPs calcined at the temperature of 400 °C. Furthermore, the photocatalytic activity of FST-N NCPs decreases to 32±1.5 % with increasing calcination temperature from 400 to 500 °C. Using the FST-N NCPs (0.8 g/L) calcined at 400 °C, phenol (C_0=100 mg/L) degradation percent after 480 min irradiation were 37±1.5, 46±1.5, and 33±1.5 % at pH 3, 7, and 11, respectively. The results of visible-active magnetic catalyst reuse showed the effectiveness of prepared samples after 10 cycles of repetitive use with degradation rate of 88.88 % of the first run, indicating the promising recyclability and photochemical stability of FST-N composite NCPs. The nanocomposites synthesized in this study could have the potential to be utilized as promising cost-effective and environmentally friendly materials in degradation of hazardous environmental organic pollutants prior to biological treatment processes in industrial-scale water and wastewater treatment systems.

References

Abramson S, Srithammavanh L, Siaugue JM, Horner O, Xu X, Cabuil V (2009) Nanometric core-shell-shell γ-Fe_2O_3/SiO_2/TiO_2 particles. J Nanoparticle 11:459–465

Arana J, Rendon TR, Rodriguez JMD, Melian JAH, Diaz OG, Perez J (2001) Highly concentrated phenolic wastewater treatment by the photo-Fenton reaction, mechanism study by FTIR-ATR. J Chemosphere 44:1017–1023

Behnajady MA, Eskandarloo H, Modirshahla N, Shokri M (2011) Investigation of the effect of sol–gel synthesis variables on structural and photocatalytic properties of TiO_2 nanoparticles. J Desalination 278:10–17

Beydoun D, Amal R (2002) Implications of heat treatment on the properties of a magnetic iron oxide–titanium dioxide photocatalyst. J Mater Sci Eng 94:71–81

Beydoun D, Amal R, Low GKC, McEvoy S (2000) Novel photocatalyst: titania-coated magnetite activity and photodissolution. J Phys Chem B 104:4387–4396

Beydoun D, Amal R, Scott J, Low G, McEvoy S (2001) Studies on the mineralization and separation efficiencies of a magnetic photocatalyst. Chem Eng Technol 24:745–748

Beydoun D, Amal R, Low GKC, McEvoy S (2002) Occurrence and prevention of photodissolution at the phase junction of magnetite and titanium dioxide. J Mol Catal A Chem 180:193–200

Burda C, Lou Y, Chen X, Samia ACS, Stout J, Gole JL (2003) Enhanced nitrogen doping in TiO_2 nanoparticles. J Nano Lett 3:1049–1051

Calza P, Sakkas VA, Medana C, Baiocchi C, Dimou A, Pelizzetti E, Albanis T (2006) Photocatalytic degradation study of diflofenac over aqueous TiO_2 suspensions. Appl Catal B 67:197–205

Cano M, Sbargoud K, Allard E, Larpent C (2012) Magnetic separation of fatty acids with iron oxide nanoparticles and application to extractive deacidification of vegetable oils. J Green Chem 14:1786–1795

Carp O, Huisman CL, Reller A (2004) Photoinduced reactivity of titanium dioxide. Prog Solid State Chem 32:33–177

Chang CF, Tseng IP (2013) Degradation of phenol by using magnetic photocatalysts of titania. Water Sci Technol 67:1434–1441

Chen XB, Burda C (2004) Photoelectron spectroscopic investigation of nitrogen-doped titania nanoparticles. J Phys Chem B 108:15446–15449

Cheng X, Yu X, Xing Z (2012) Characterization and mechanism analysis of N doped TiO_2 with visible light response and its enhanced visible activity. J Appl Surf Sci 258:3244–3248

Chi Y, Yuan Q, Li Y, Tu J, Zhao L, Li N, Li X (2012) Synthesis of Fe_3O_4@SiO_2-Ag magnetic nanocomposite based on small-sized and highly dispersed silver nanoparticles for catalytic reduction of 4-nitrophenol. J Colloid Interface Sci 383:96–102

Demir N, Gündüz G, Dükkancı M (2015) Degradation of a textile dye, Rhodamine 6G (Rh6G), by heterogeneous sonophotoFenton process in the presence of Fe-containing TiO_2 catalysts. Environ Sci Pollut Res 22:3193–3201

Deng YH, Qi DW, Deng CH, Zhang XM, Zhao DY (2007) Superparamagnetic high-magnetization microspheres with an Fe_3O_4@SiO_2 core and perpendicularly aligned mesoporous SiO_2 shell for removal of microcystins. J Am Chem Soc 130:28–29

Devi LG, Rajashekhar KE (2011) A kinetic model based on non-linear regression analysis is proposed for the degradation of phenol under UV/solar light using nitrogen doped TiO_2. J Mol Catal A Chem 334:65–76

Ding Z, Lu GQ, Greenfield PF (2000) Role of the crystallite phase of TiO_2 in heterogeneous photocatalysis for phenol oxidation in water. J Phys Chem B 104:4815–4820

Dubey N, Rayalu SS, Labhsetwar NK, Devotta S (2008) Visible light active zeolite-based photocatalysts for hydrogen evolution from water. Int J Hydrog Energy 33:5958–5966

Fernández-Ibáñez P, Blanco J, Malato S, de las Nieves FJ (2003) Application of the colloidal stability of TiO_2 particles for recovery and reuse in solar photocatalysis. J Water Res 37:3180–3188

Gao J, Jiang R, Wang J, Wang B, Li K, Kang P, Li Y, Zhang X (2011) Sonocatalytic performance of Er^{3+}:$YAlO_3$/TiO_2–Fe_2O_3 in organic dye degradation. Chem Eng J 168:1041–1048

Geng J, Yang D, Zhu J, Chen D, Jiang Z (2009) Nitrogen-doped TiO_2 nanotubes with enhanced photocatalytic activity synthesized by a facile wet chemistry method. J Mater Res Bull 44(1):146–150

Gorska P, Zaleska A, Kowalska E, Klimczuk T, Sobczak JW, Skwarek E, Janusz W, Hupka J (2008) TiO_2 photoactivity in vis and UV light: the influence of calcinations temperature and surface properties. Appl Catal B 84:440–447

Hu S, Wang A, Li X, Löwe H (2010) Hydrothermal synthesis of well-dispersed ultrafine N-doped TiO_2 nanoparticles with enhanced photocatalytic activity under visible light. J Phys Chem Solids 71:156–162

Hurum DC, Gray KA, Rajh T, Thurnauer MC (2005) Recombination pathways in the Degussa P25 formulation of TiO2: surface versus lattice mechanisms. J Phys Chem B 109:977–980

Jing J, Liu M, Colvin VL, Li W, Yu WW (2011) Photocatalytic degradation of nitrogen-containing organic compounds over TiO_2. J Mol Catal A Chem 351:17–28

Jing J, Li J, Feng J, Li W, Yu WW (2013) Photodegradation of quinoline in water over magnetically separable Fe_3O_4/TiO_2 composite photocatalysts. J Chem Eng 219:355–360

Jung KY, Park SB (2000) Enhanced photoactivity of silica-embedded titania particles prepared by sol-gel process for the decomposition of trichloroethylene. Appl Catal B 25:249–256

Kalantari M, Kazemeini M, Arpanaei A (2013) Facile fabrication and characterization of amino-functionalized Fe_3O_4 cluster@SiO_2 core/shell nanocomposite spheres. Mater Res Bull 48:2023–2028

Kim G, Choi W (2010) Charge-transfer surface complex of EDTA-TiO_2 and its effect on photocatalysis under visible light. Appl Catal B Environ 100:77–83

Kumar R, De U, Prasad R (2006) Physical and chemical response of 70 MeV carbon ion irradiated polyether sulphone polymer. Nucl Instrum Methods Phys Res Sect B Beam Interact Mater Atoms 248:279–283

Lettmann C, Hildenbrand K, Kisch H (2001) Visible lightphotodegradation of 4-chlorophenol with a coke-containing titanium dioxide photocatalyst. Appl Catal B 32(4):215–227

Li Y, Lee NH, Song JS, Lee EG, Kim SJ (2005) Synthesis and photocatalytic properties of nano bi-crystalline titania of anatase and brookite by hydrolyzing $TiOCl_2$ aqueous solution at low temperatures. Res Chem Intermed 31:309–318

Li Y, Ma M, Wang X, Wang X (2008) Inactivated properties of activated carbon-supported TiO_2 nanoparticles for bacteria and kinetic study. J Environ Sci 20:1527–1533

Lindgren T, Mwabora JM, Avendao E, Jonsson J, Hoel A, Granqvist CG, Lindquist SE (2003) Photoelectrochemical and optical properties of nitrogen doped titanium dioxide films prepared by reactive DC magnetron sputtering. J Phys Chem B 107(24):5709–5716

Liu Y, Chen L, Hu J, Li J, Richards R (2010) TiO_2 nanoflakes modified with gold nanoparticles as photocatalysts with high activity and durability under near UV irradiation. J Phys Chem C 114:1641–1645

Liu H, Jia Z, Ji S, Zhang Y, Li M, Yang H (2011) Synthesis of TiO_2/SiO_2@Fe_3O_4 magnetic microspheres and their properties of photocatalytic degradation dyestuff. Catal Today 175:293–298

Liu G, He F, Zhang J, Li L, Li F, Chen L, Huang Y (2014a) Yolk–shell structured Fe3O4@C@F-TiO_2 microspheres with surface fluorinated as recyclable visible-light driven photocatalysts. Appl Catal B 150–151:515–522

Liu Z, Liu X, Lu D, Fang P, Wang S (2014b) Grape-like Bi2WO6/TiO_2 hierarchical microspheres: a superior visible light photocatalyst with magnetic recycling property. Mater Lett 130:143–145

Lucas MS, Peres JA (2006) Decolorization of the azo dye reactive black 5 by Fenton and photo-Fenton oxidation. Dyes Pigments 71:236–244

Matsumoto T, Iyi N, Kaneko Y, Kitamura K, Ishihara S, Takasu Y, Murakami Y (2007) High visible-light photocatalytic activity of

nitrogen-doped titania prepared from layered titania/isosterate nanocomposite. Catal Today 120:226–232

Paola AD, Cufalo G, Addamo M, Bellardita M, Campostrini R, Ischia M, Ceccato R, Palmisano L (2008) Photocatalytic activity of nanocrystalline TiO_2 (brookite, rutile and brookite-based) powders prepared by thermohydrolysis of $TiCl_4$ in aqueous chloride solutions. Colloids Surf A Physicochem Eng Asp 317:366–376

Parsons S (2004) Advanced oxidation processes for water and wastewater treatment. IWA Publishing, Cornwall

Ren C, Qiu W, Chen Y (2013) Physicochemical properties and photocatalytic activity of the TiO_2/SiO_2 prepared by precipitation method. Sep Purif Technol 107:264–272

Sakthivel S, Janczarek M, Kisch H (2004) Visible light activity and photoelectrochemical properties of nitrogen-doped TiO_2. J Phys Chem B 108:19384–19387

Sanchez FG, Diaz AN, Garcia JA (1995) P-phenol derivatives as enhancers of the chemiluminescent luminol-horseradish peroxidase-H_2O_2 reaction: substituent effects. J Lumin 65:33–39

Sathish M, Viswanathan B, Viswanath RP, Gopinath CS (2005) Synthesis, characterization, electronic structure, and photocatalytic activity of nitrogen-doped TiO_2 nanocatalyst. Chem Mater 17:6349

Serpone N, Lawless D, Khairutdinov R (1995) size effects on the photophysical properties of colloidal anatase TiO_2 particles: size quantization versus direct transitions in this indirect semiconductor. J Phys Chem 99:16646–16654

Shao G, Zhang X, Yuan Z (2008) Preparation and photocatalytic of hierarchically mesoporous-macroporous TiO_2-xNx. Appl Catal B 82: 208–218

Swan P, Walker RM, Wopenka B, Freeman JJ (1981) 3.4 μm absorption in interplanetary dust particles: evidence for indigenous hydrocarbons and a further link to comet Halley. J Meteoritics 22:510

Treschev SY, Chou PW, Tseng YH, Wang JB, Perevedentseva EV, Cheng CL (2008) Photoactivities of the visible-light-activated mixed-phase carbon-containing titanium dioxide: the effect of carbon incorporation. Appl Catal B 79:8–16

Valentin CD, Finazzi E, Pacchioni G, Selloni A, Livraghi S, Paganini MC, Giamello E (2007) N-doped TiO_2: theory and experiment. J Chem Phys 339:44–56

Venkatachalam N, Palanichamy M, Murugesan V (2007) Sol–gel preparation and characterization of alkaline earth metal doped nano TiO2: efficient photocatalytic degradation of 4-chlorophenol. J Mol Catal A Chem 273:177–185

Wang CC, Zhang Z, Ying JY (1997) Photocatalytic decomposition of halogenated organics over nanocrystalline titania. Nanostruct Mater 9:583–586

Wang Z, Cai W, Hong X, Zhao X, Xu F, Cai C (2005) Photocatalytic degradation of phenol in aqueous nitrogen-doped TiO_2 suspensions with various light sources. Appl Catal B 57:223–231

Wang C, Yin L, Zhang L, Kang L, Wang X, Gao R (2009) Magnetic (γ-$Fe_3O_4@SiO_2)_n@TiO_2$ functional hybrid nanoparticles with active photocatalytic ability. J Phys Chem C 113:4008–4011

Wang E, He T, Zhao L, Chen Y, Gao Y (2010) Improved visible light photocatalytic activity of titania doped with tin and nitrogen. J Mater Chem 21:144–150

Wang P, Zhou T, Wang R, Lim TT (2011a) Carbon-sensitized and nitrogen-doped TiO_2 for photocatalytic degradation of sulfanilamide under visible-light irradiation. Water Res 45:5015–5026

Wang P, Yap P, Lim TT (2011b) C–N–S tridoped TiO_2 for photocatalytic degradation of tetracycline under visible-light irradiation. Appl Catal A 399:252–261

Wang Y, Zhao H, Gao J, Zhao G, Zhang Y, Zhang Y (2012) Rapid mineralization of azodye wastewater by microwave synergistic electro-Fenton oxidation process. J Phys Chem C 116:7457–7463

Wu Q, Ouyang J, Xie K, Sun L, Wang M, Lin C (2012) Ultrasound-assisted synthesis and visible-light-driven photocatalytic activity of Fe-incorporated TiO_2 nanotube array photocatalysts. J Hazard Mater 199–200:410–417

Xu J, Dai W, Li J, Cao Y, Li H, He H, Fan K (2008) Simple fabrication of thermally stable apertured N-doped TiO_2 microtubes as a highly efficient photocatalyst under visible light irradiation. J Catal Commun 9:146–152

Xuan S, Jiang W, Gong X, Hu Y, Chen Z (2008) Magnetically separable Fe_3O_4/TiO_2 hollow spheres: fabrication and photocatalytic activity. J Phys Chem 113:553–558

Yap PS, Lim TT, Srinivasan M (2011) Nitrogen- doped TiO_2/AC bifunctional composite prepared by two-stage calcination for enhanced synergistic removal of hydrophobic pollutant using solar irradiation. J Catal Today 161:46–52

Yu XX, Yu J, Cheng B, Jaroniec M (2009) Synthesis of hierarchical flower-like AlOOH and TiO_2/AlOOH superstructures and their enhanced photocatalytic properties. J Phys Chem C 113:17527–17535

Zhang J, Zhang L, Zhou S, Chen H, Zhong H, Zhao Y, Wang X (2014) Magnetically separable attapulgite−TiO2−FexOy composites with superior activity towards photodegradation of methyl orange under visible light radiation. Ind Eng Chem 20:3884–3889